Journal of *Marine Science and Engineering*

MDPI

Article

Stress Concentration Factors Due to Misalignment at Girth Welds in Bi-Layer Pipes

Ruili Guo [1], Hongyang Hu [2], Haisheng Zhao [3] and Yao Zhang [2,*]

[1] School of Civil Engineering and Architecture, Wuhan Institute of Technology, Wuhan 430074, China; 20120103@wit.edu.cn
[2] School of Architecture and Civil Engineering, Xiamen University, Xiamen 361005, China; 25320221152407@stu.xmu.edu.cn
[3] State Key Laboratory of Coastal and Offshore Engineering, Dalian University of Technology, Dalian 116024, China; hzhao@dlut.edu.cn
* Correspondence: zhangyao@xmu.edu.cn

Abstract: In recent years, bi-layer pipes, composed of an inner layer and an outer layer, have been widely used in offshore engineering. In this study, the governing equation for a bi-layer pipe subjected to axisymmetric loadings is derived based on classical shell theory. Then, the equation is used to develop stress concentration factor formulations for girth welds in bi-layer pipes with fabrication tolerances and thickness transitions. Axisymmetric finite element analysis is carried out to verify the accuracy of the proposed formulations. It is noted that these formulations can be well suited for determining the stress concentration factors for a wide range of thickness ratios (ratio of the inner layer thickness to the total thickness in a bi-layer pipe) varying from 0.0 to 1.0. They can also obtain accurate stress concentration factors whether the elastic modulus of the inner layer is smaller or larger than that of the outer layer.

Keywords: bi-layer pipe; finite element analysis; classical shell theory; stress concentration factor

Citation: Guo, R.; Hu, H.; Zhao, H.; Zhang, Y. Stress Concentration Factors Due to Misalignment at Girth Welds in Bi-Layer Pipes. *J. Mar. Sci. Eng.* **2024**, *12*, 231. https://doi.org/10.3390/jmse12020231

Academic Editor: Bruno Brunone

Received: 7 January 2024
Revised: 22 January 2024
Accepted: 26 January 2024
Published: 28 January 2024

1. Introduction

Misalignment widely exists in welded structures due to the eccentricities at fabrication tolerances or thickness transitions. The presence of misalignment introduces local bending stress at the welded joints, and in turn, the additional loading increases the stress of the structures. A stress concentration factor (SCF) [1] is used to assess quantitatively the effect of misalignment on the failures of structures, and it is defined as:

$$\mathrm{SCF} = 1 + \frac{\sigma_s}{\sigma_{nom}} \tag{1}$$

where σ_s is the maximum induced bending stress due to misalignment and σ_{nom} is the nominal stress. The maximum stress, often referred to as the hot spot stress, is the sum of the maximum bending stress and the nominal stress. The hot spot stress, in combination with S-N data, is usually used for the fatigue life evaluation of structures subjected to dynamic loadings, and it is determined using the SCF multiplying the nominal stress. Therefore, it is necessary to calculate the SCFs for various plated and tubular structural members, and considerable research has been carried out to determine the SCFs [2–6]. Maddox [7] performed the derivation of SCFs at transverse butt welds under fatigue loadings. Based on extensive finite element (FE) analysis of various tubular configurations, a set of SCF formulations for the most commonly used tubular joints was developed by Efthymiou [8] and Smedley and Fischer [9]. Lotsberg [10–12] conducted a detailed assessment of SCFs for butt welds in plated and tubular structures subjected to axial force and internal pressure using the classical shell theory [13]. Effects of fabrication tolerances, thickness transitions and ring-stiffeners on SCFs were investigated systematically. It is

noted that these formulations are used to calculate the SCFs of homogeneous (one-layer) plated or tubular structures and have been incorporated into fatigue design rules such as DNV-RP-C203 [14] and BS 7910:2013 [15].

In recent years, bi-layer pipes, consisting of two layers with different functions for each layer, have been widely used to satisfy special needs [16,17]. For example, high-quality bi-layer pipelines are increasingly emerging as the most efficient mode of transporting vital energy resources such as oil and gas as extensive installation takes place [18–20]. The clad pipe is one of these cases, which is composed of a carbon steel outer pipe and a corrosion resistant alloy liner, protecting the outer pipe from corrosion. Despite the numerous numerical schemes [21–23] developed for assessing the fatigue and fracture behaviour of bi-layer pipes with misalignment at girth welds, their practical application remains challenging due to the difficulty of generating FE models in engineering settings. The SCF formulations, as mentioned earlier, encounter limitations when directly applied to evaluate stress concentrations in the notch regions at both the inner and outer sides of bi-layer pipes.

To overcome these challenges, this study adopts an innovative approach by initially deriving the governing equation for a bi-layer cylindrical shell under axisymmetric loadings, utilizing the principles of classical shell theory. This derived equation serves as the cornerstone for developing SCF formulations tailored explicitly for girth welds in bi-layer pipes, accounting for fabrication tolerances and thickness transitions. The efficacy and reliability of these formulations are rigorously validated through comprehensive axisymmetric FE analyses, ensuring their accuracy and applicability in real-world engineering scenarios. The developed models not only enhance the understanding of the fatigue and fracture behavior in bi-layer pipes but also provide a practical and robust tool for engineers dealing with complex structural assessments in the field.

2. Derivation of Governing Equation for a Bi-Layer Cylindrical Shell

A one-layer cylindrical shell subjected to the forces distributed symmetrically with respect to the axis of the cylinder is frequently encountered in practice. The governing equation for the shell has been built up using the classical shell theory [13]. In this study, a bi-layer cylindrical shell under the same loading conditions (Figure 1) is considered, and the corresponding governing equation is derived as an extension to the classical shell theory [13] (please refer to Appendix A for details). The definitions of related parameters used in Figure 1 are given in Table 1.

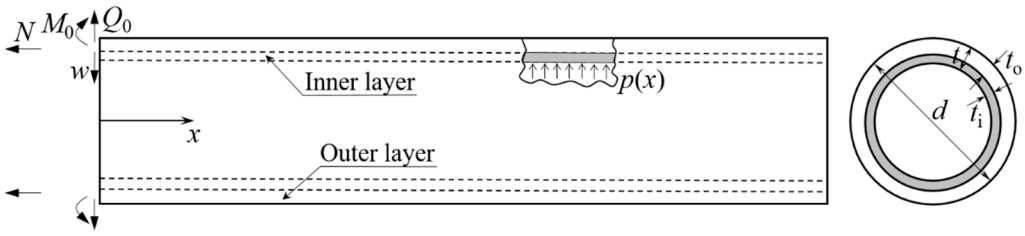

Figure 1. Bi-layer cylindrical shell subjected to symmetric loadings with respect to its axis.

Table 1. Definition of parameters.

Layers	Thickness	Outer Diameter	Radius	Elastic Modulus	Poisson's Ratio
Inner layer	t_i	$d - t_o$	/	E_i	v_i
Outer layer	t_o	d	/	E_o	v_o
Bi-layer pipe	$t = t_i + t_o$	d	$r = \frac{d-t}{2}$	/	/

The governing equation of the bi-layer shell presented in Appendix A is:

$$D_b \frac{d^4 w}{dx^4} + \frac{\alpha E_o t}{r^2} w = p(x) - \frac{v}{r} N \tag{2}$$

where D_b is the flexural rigidity of the bi-layer shell, α is a constant depending on the ratio of inner layer thickness to the total thickness and the ratio of elastic modulus of the inner layer to the elastic modulus of the outer layer, r is the radius of the bi-layer pipe, v is the Poisson's ratio for both inner layer and outer layer, and N is the axial force applied on the pipe. More details about D_b and α can be referred to in Appendix A.

By introducing the notation,

$$\beta^4 = \frac{\alpha E_o t}{4 r^2 D_b} \tag{3}$$

Equation (2) can be expressed in the following simplified form:

$$\frac{d^4 w}{dx^4} + 4\beta^4 w = \frac{p(x)}{D_b} - \frac{v}{r D_b} N \tag{4}$$

The general solution of Equation (4), w, consists of a homogeneous part, w_h, and a particular part (w_p), and it is expressed as:

$$w = w_h + w_p \tag{5}$$

The homogeneous part of the solution is

$$w_h = \frac{e^{-\beta x}}{2\beta^3 D_b} \{\beta M_0 [\cos(\beta x) - \sin(\beta x)] + Q_0 \cos(\beta x)\} \tag{6}$$

where M_0 and Q_0 are the bending moment and the shear force per unit circumferential length at $x = 0$, as shown in Figure 1.

Using the following notation,

$$\varphi(\beta x) = e^{-\beta x} [\cos(\beta x) + \sin(\beta x)] \tag{7a}$$

$$\psi(\beta x) = e^{-\beta x} [\cos(\beta x) - \sin(\beta x)] \tag{7b}$$

$$\theta(\beta x) = e^{-\beta x} \cos(\beta x) \tag{7c}$$

$$\zeta(\beta x) = e^{-\beta x} \sin(\beta x) \tag{7d}$$

Equation (6) can be written as:

$$w_h = \frac{1}{2\beta^3 D_b} [\beta M_0 \psi(\beta x) + Q_0 \theta(\beta x)] \tag{8}$$

The particular part of the general solution of Equation (5) is:

$$w_p = \frac{r}{\beta E_0 t} [r p(x) - v N] \tag{9}$$

For constant p, the slope at a section x can be obtained by differentiating Equation (6), and this provides:

$$\frac{\partial w}{\partial x} = -\frac{1}{2\beta^2 D_b} [2\beta M_0 \theta(\beta x) + Q_0 \varphi(\beta x)] \tag{10}$$

The moment (per unit circumferential length) at a section x is determined by the following expression:

$$M_x = -D_b \frac{\partial^2 w}{\partial x^2} = \frac{1}{\beta}[\beta M_0 \varphi(\beta x) + Q_0 \zeta(\beta x)] \tag{11}$$

The shear force (per unit circumferential length) at a section x is calculated as:

$$Q_x = \frac{\partial M_x}{\partial x} = -[2\beta M_0 \zeta(\beta x) - Q_0 \psi(\beta x)] \tag{12}$$

3. Girth Welds in Bi-Layer Pipes with Fabrication Tolerances

In this section, a stress concentration in the girth weld of a bi-layer pipe with an eccentricity e as shown in Figure 2a is analyzed using the equation obtained in Section 2. Figure 2b shows the geometry analyzed. The length of the girth weld is L, and the corresponding slope is α. The pipe is subjected to an axial loading per unit circumferential length N. Due to the asymmetry of the static model, the moment at the middle of the weld ($x = 0$) is zero (inflection point), and the moments at the notch region ($x = \pm L/2$) have the same values ($Ne/2$) but different directions, as shown in Figure 2c.

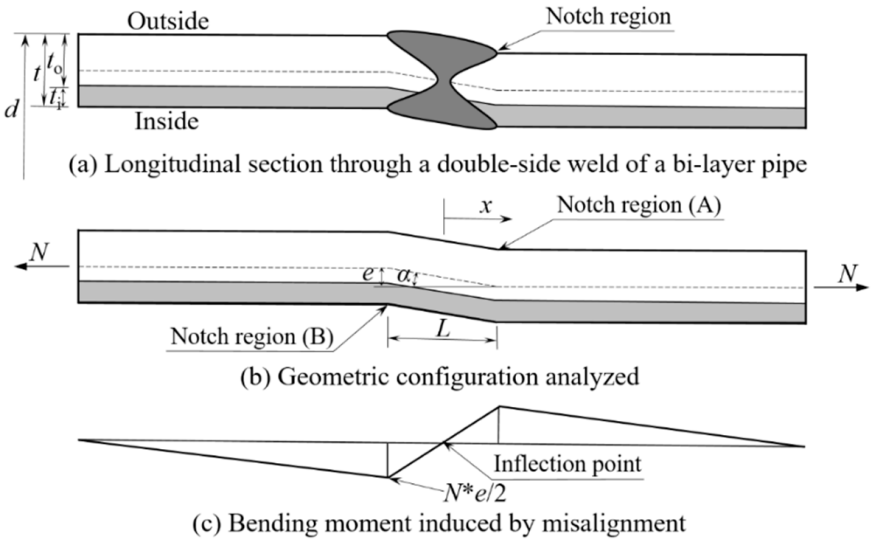

Figure 2. Model of a bi-layer pipe with fabrication tolerance over a section length L.

The boundary conditions of the bi-layer pipe shown in Figure 2b can be written as:

$$M|_{x=0} = 0, \; Q|_{x=0} = -N\sin(\alpha) \cong -N\frac{e}{L} \tag{13}$$

On the other hand, according to Equation (11), the bending moment at $x = L/2$ is:

$$M|_{x=\frac{L}{2}} = -\frac{Ne}{\beta L} e^{-\frac{\beta L}{2}} \sin\left(\frac{\beta L}{2}\right) \tag{14}$$

In this study, the notch region considered is on the outside of the pipe indicated by "A" in Figure 2b. Hence, the bending stress induced by misalignment at "A" is:

$$\sigma_b^A = \frac{E_o Ne(t - 2\eta_n)}{2(1 - v^2) D_b \beta L} e^{-\frac{\beta L}{2}} \sin\left(\frac{\beta L}{2}\right) \tag{15}$$

The nominal stress for the bi-layer pipe without misalignment needs to be determined in order to calculate the SCF. In Appendix A, it is assumed that the outer and the inner

layers of the aligned pipe undergo the same deformation when subjected to an axial loading N. Hence, the nominal stress is expressed as:

$$\sigma_{nom}^{A} = \frac{N}{(1-\bar{t}+\bar{t}\overline{E})t} \tag{16}$$

where $\bar{t}$ is the ratio of inner layer thickness to the total thickness, and $\overline{E}$ is the ratio of the elastic modulus of the inner layer to the elastic modulus of the outer layer.

Based on Equations (15) and (16), the SCF at "A" is determined:

$$\mathrm{SCF} = \frac{\sigma_{nom}^{A} + \sigma_{b}^{A}}{\sigma_{nom}^{A}} = 1 + \frac{3.22\mu}{(1-v^2)^{1/4}}\frac{e}{L}\sqrt{\frac{d-t}{t}}\mathrm{e}^{-\frac{\beta L}{2}}\sin\left(\frac{\beta L}{2}\right) \tag{17}$$

where

$$\mu = \frac{\left(1-2\bar{t}+\bar{t}^2+2\bar{t}\overline{E}-\bar{t}^2\overline{E}\right)\sqrt{1-\bar{t}+\bar{t}\overline{E}}}{\left(1-4\bar{t}+4\bar{t}\overline{E}+6\bar{t}^2-6\bar{t}^2\overline{E}-4\bar{t}^3+4\bar{t}^3\overline{E}+\bar{t}^4-2\bar{t}^4\overline{E}+\bar{t}^4\overline{E}^2\right)^{3/4}} \tag{18}$$

When the Poisson's ratio is set as 0.3 ($v = 0.3$), Equation (17) can be written as:

$$\mathrm{SCF} = 1 + 3.30\mu\frac{e}{L}\sqrt{\frac{d-t}{t}}\mathrm{e}^{-\frac{\beta L}{2}}\sin\left(\frac{\beta L}{2}\right) \tag{19}$$

The above expression is the same with the formulation derived by Lotsberg [10] for double-sided circumferential welds in tubular members except the remaining dimensionless parameter μ accounting for the varying thickness ratio $\bar{t}$ and elastic property ratio $\overline{E}$. When $\bar{t} = 0$ or $\overline{E} = 1$, $\mu = 1$, and Equation (19) for calculating the SCF of a misaligned bi-layer pipe is degraded to the formulation for a one-layer pipe given by Lotsberg [10], verifying the validity of Equation (19) derived in this study to some extent.

The comparison of the SCFs obtained by FE analysis and Equation (19) is carried out to further demonstrate the accuracy of the formulation. The mesh design of the FE models is based on the recommendations for the notch stress methodology in Appendix D of DNV-RP-C203 [14]. The notches at "A" and "B" are modeled using a radius of 1.0 mm. An axisymmetric pipeline model with a diameter of 400 mm and thickness of 20 mm is analyzed in this study.

At first, the SCFs obtained by FE analysis for a misaligned one-layer pipe are compared with that given by Lotsberg [10] formulation to test the validity of FE models (Figure 3). It is observed that the maximum percentage difference of SCFs is 1.2% ($e/t = 0.15$), illustrating a good agreement between the FE results and the formulation. Hence, the FE models are considered suitable for numerical analysis of a misaligned bi-layer pipe when adequate elements are used to obtain good convergence. The convergent test shows that a total of nearly 1×10^4 elements is adequate in this study.

Figure 4 compares the SCFs from Equation (19) and FE analysis for varying e/t ($0.00 \leq e/t \leq 0.15$) and $\overline{E}$ ($\overline{E} = 0.5$ and 2.0) with constant $\bar{t}$ ($\bar{t} = 0.5$), showing a very good correlation between the two results. As the misalignment increases, the value of SCF also increases. FE analyses and formula-based calculations show consistency in the overall trend. However, it is observable that compared to FE results, the outcomes derived from formulas are slightly conservative. The reason might be that it is assumed that the shell has infinite curvature radius or the ratio of thickness to radius can be neglected in the theoretical derivation; however, the curvature radius is not infinite, and the ratio of thickness to radius is not zero although it is quite near zero in the FE models. Overall, both methods exhibit a very good correlation. This alignment in trends between the two approaches underscores the reliability of the derived formular in predicting the impact of misalignment on SCF in engineering applications.

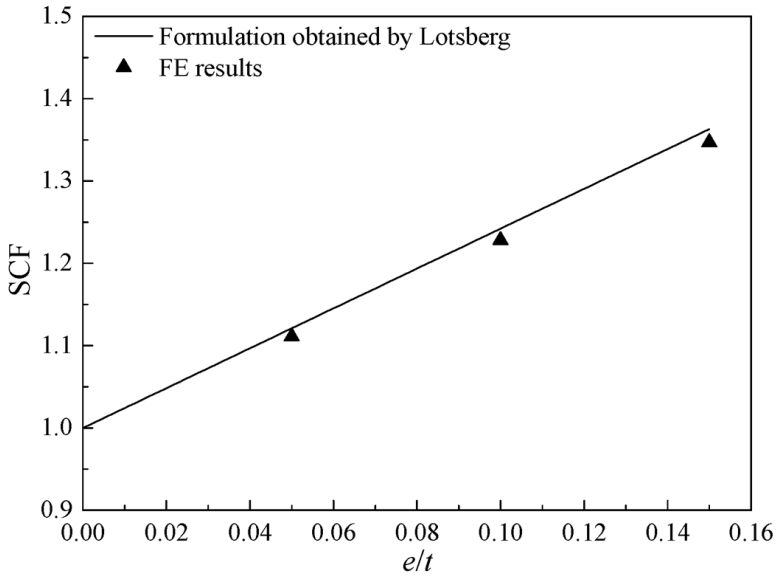

Figure 3. Comparison of SCFs from FE analysis and Lotsberg's formulation.

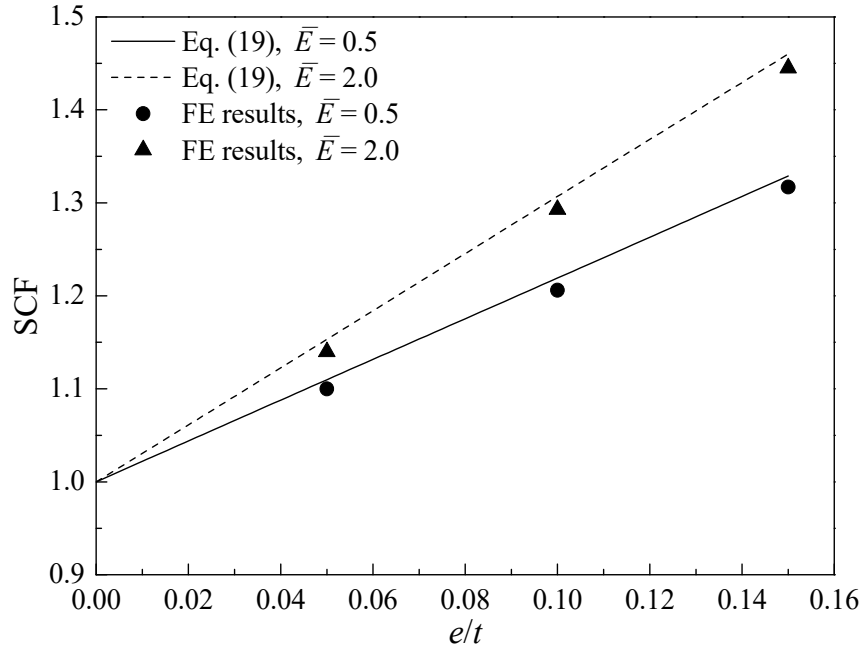

Figure 4. Comparison of SCFs from Equation (19) and FE analysis for $\bar{t} = 0.5$.

For varying $\bar{t}$ with constant e/t $(= 0.15)$ and $\overline{E}$ $(= 0.5)$, a good agreement between Equation (19) and FE results is also observed, as indicated in Figure 5. Therefore, Equation (19) can accurately assess the stress concentration in the notch region of the girth weld in a bi-layer pipe.

Figure 6 shows the influence of $\overline{E}$ with the variation of $\bar{t}$ on the SCF given by Equation (19) for constant e/t $(= 0.15)$. $\overline{E} = 1$ indicates that the inner layer and the outer layer in the bi-layer pipe have the same elastic modulus, which is the case of the one-layer pipe. Hence, the SCF is not affected by the varying $\bar{t}$ as presented by a horizontal line in Figure 6. $\overline{E} > 1$ means the elastic modulus of the inner layer is higher than that of the outer layer, and a larger $\overline{E}$ raises a more pronounced effect on the SCF. For the case of $\overline{E} < 1$, a reverse trend is observed in comparison with that of $\overline{E} > 1$.

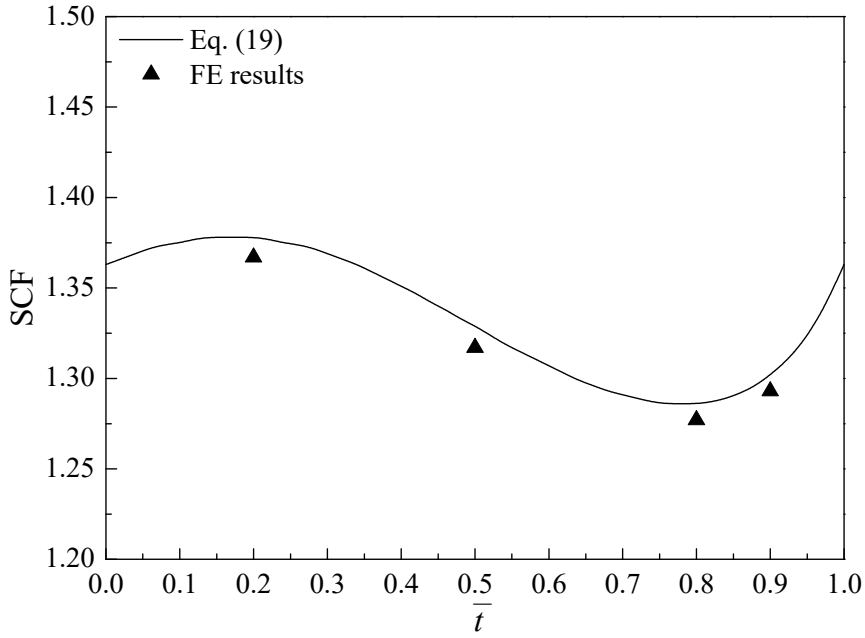

Figure 5. Comparison of variation of SCFs over $\bar{t}$ from Equation (19) and FE analysis for $e/t = 0.15$ and $\overline{E} = 0.5$.

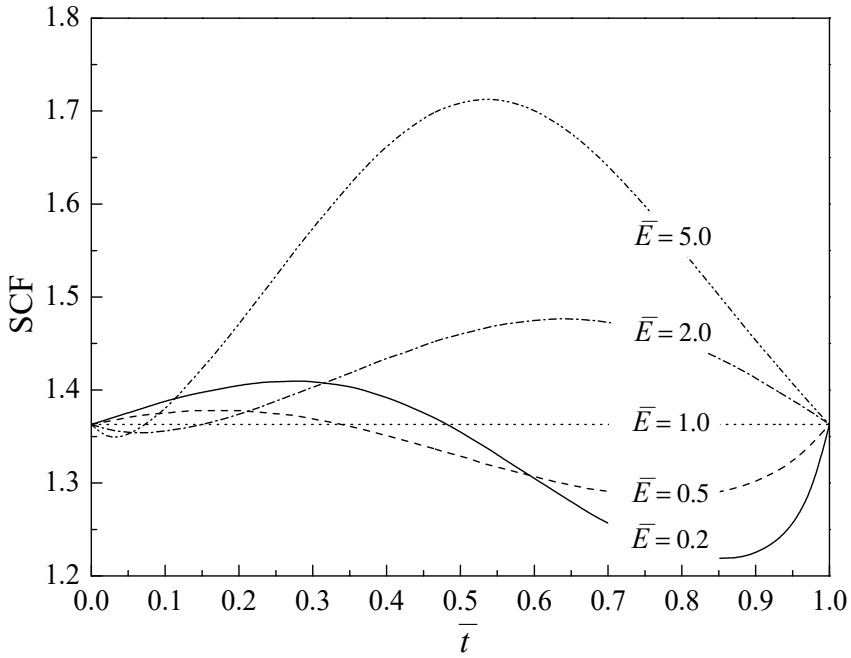

Figure 6. Effect of $\overline{E}$ on SCF over $\bar{t}$ for $e/t = 0.15$.

Even though it has been indicated that Equation (19) is used to calculate the SCF at the notch region "A", it can be transformed into determining the SCF at "B" (Figure 2b) by substituting the two dimensionless parameters $(1 - \bar{t})$ and $1/\overline{E}$ into Equation (19) instead of $\bar{t}$ and $\overline{E}$. Figure 7 shows the calculation of the SCF at "B" for $\overline{E} = 2.0$ and $e/t = 0.15$ based on the above approach. The two parameters $(1 - \bar{t})$ and $1/\overline{E}$ $(= 0.5)$ are substituted into Equation (19) and the plot of SCF over $\bar{t}$ for "B" is given using a dashed line in Figure 7. It is noted that the two lines for "A" and "B" are symmetric with $\bar{t} = 0.5$, and the validity of the above transform approach is further verified using the FE analysis as indicated by the triangle symbol in Figure 7.

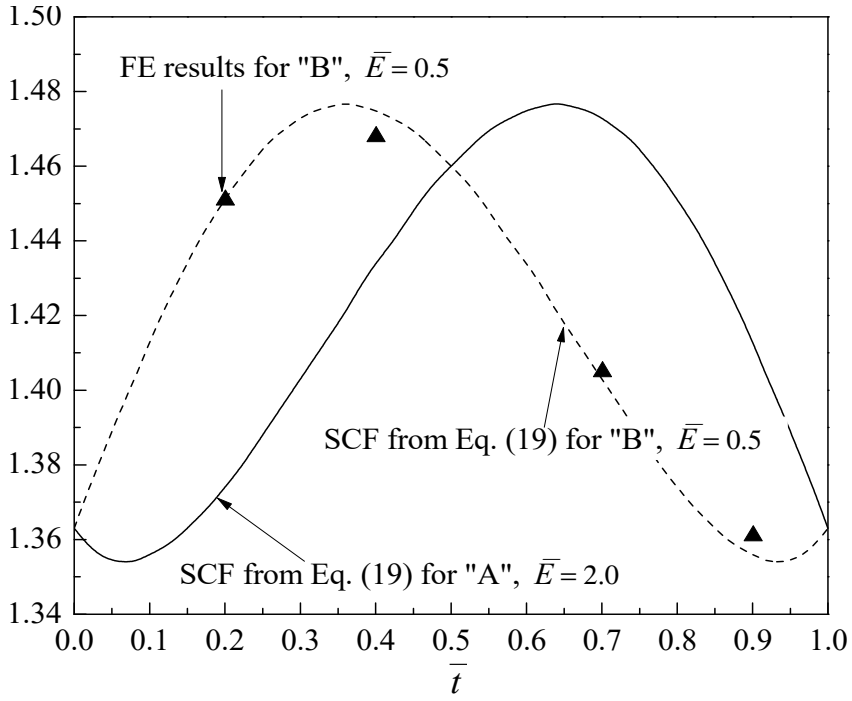

Figure 7. Calculation of SCF at notch region "B" based on that of "A" for $e/t = 0.15$.

The SCF formulation in Equation (19) is derived based on the double-side weld configuration of the bi-layer pipe with centerline offset misalignment. However, the formulation can also be applied to determine the SCF at the pipe's notch region "A" with single-side welds (Figure 8). The SCF at "B" becomes close to 1.0 due to the region close to the intersection point where the bending moment induced by misalignment is zero.

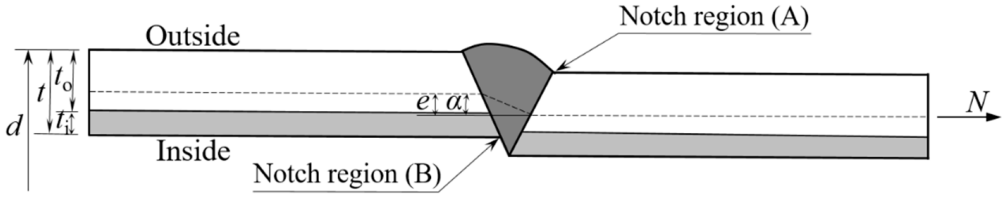

Figure 8. Longitudinal section through single-side welds of a bi-layer pipe.

4. Girth Welds in Bi-Layer Pipes at Thickness Transitions

This section details the derivation of the SCF in the girth weld of a bi-layer pipe with thickness transitions, as shown in Figure 9.

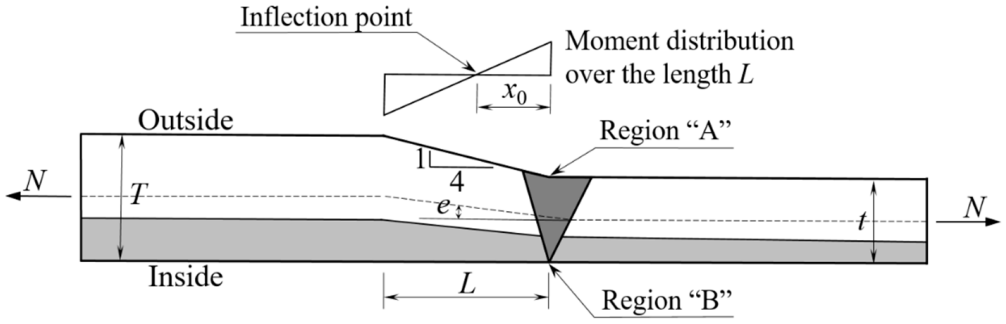

Figure 9. Longitudinal section of a bi-layer pipe with thickness transitions.

For the pipes subjected to dynamic loading, thickness transitions are normally to be fabricated with slope 1:4. The inflection point (zero moment) in Figure 9 needs to be determined in advance in order to calculate the eccentricity moment at the notch region of the girth weld based on Equation (11). It is assumed that the thickness ratio $\bar{t}$ keeps constant along the longitudinal section of the pipe. Thus, the rotational stiffness is in proportion to the pipe thickness t raised in a power of 2.5 according to Equation (10) and x_0 (please refer to Figure 9) is given as:

$$x_0 = L\frac{t^{2.5}}{t^{2.5} + T^{2.5}} \tag{20}$$

Following the same steps for calculating the SCF in Section 3, the SCF at the transition at the outside of the pipe (region "A" as indicated in Figure 9) is:

$$\text{SCF} = 1 + 6\mu_o \frac{e}{t}\frac{1}{1 + (T/t)^{2.5}}\mathrm{e}^{-\beta x_0} \tag{21}$$

where

$$\mu_o = \frac{\left(1 - 2\bar{t} + \bar{t}^2 + 2\bar{t}\overline{E} - \bar{t}^2\overline{E}\right)\left(1 - \bar{t} + \bar{t}\overline{E}\right)}{\left(1 - 4\bar{t} + 4\bar{t}\overline{E} + 6\bar{t}^2 - 6\bar{t}^2\overline{E} - 4\bar{t}^3 + 4\bar{t}^3\overline{E} + \bar{t}^4 - 2\bar{t}^4\overline{E} + \bar{t}^4\overline{E}^2\right)} \tag{22}$$

The SCF at the transition at the interior side of the pipe (region "B" as indicated in Figure 9) is:

$$\text{SCF} = 1 - 6\mu_i \frac{e}{t}\frac{1}{1 + (T/t)^{2.5}}\mathrm{e}^{-\beta x_0} \tag{23}$$

where

$$\mu_i = \frac{\left(1 - \bar{t}^2 + \bar{t}^2\overline{E}\right)\left(1 - \bar{t} + \bar{t}\overline{E}\right)}{\left(1 - 4\bar{t} + 4\bar{t}\overline{E} + 6\bar{t}^2 - 6\bar{t}^2\overline{E} - 4\bar{t}^3 + 4\bar{t}^3\overline{E} + \bar{t}^4 - 2\bar{t}^4\overline{E} + \bar{t}^4\overline{E}^2\right)} \tag{24}$$

When $\bar{t} = 0$ or $\overline{E} = 1$, μ_o and μ_i are both equal to the unit, and Equations (21) and (23) for calculating the SCF of a misaligned bi-layer pipe become the formulations for a one-layer pipe presented by Lotsberg [10], verifying the accuracy of the proposed formulations. In addition, FE analysis is carried out to further test the validity of the formulations, as done in Section 3. Figure 10 compares the SCFs from the present formulations and FE analysis. It is observed that the formulations are in good agreement with the numerical results except for the case of the SCF at region "B" for $\overline{E} = 0.5$. However, the present formulations show a trend closer to the FE results in comparison with that given by Lotsberg [10], as indicated by an arrow line in Figure 10. In general, the results obtained from the present formulations and FE analysis are consistent with one another, validating the accuracy of Equations (21) and (23) derived using the bi-layer cylindrical shell equation given in Section 2.

Figure 11 shows the effect of $\overline{E}$ on the SCFs with the increasing $\bar{t}$ for constant $T/t(= 2.0)$ at region "A" and "B". The variation trend of the SCF with the varying $\overline{E}$ presented in Figure 11a is the same as that of Figure 9 for region "A". However, a reverse trend is observed for region "B" (Figure 11b) compared with region "A" (Figure 11a), which can be easily explained by the opposite signs in Equations (21) and (23). The SCF at region "B" is minimal when region "A" has the maximum SCF value for certain dimensionless parameters $\bar{t}$ and $\overline{E}$, illustrating a reverse variation trend as shown in Figure 11a,b.

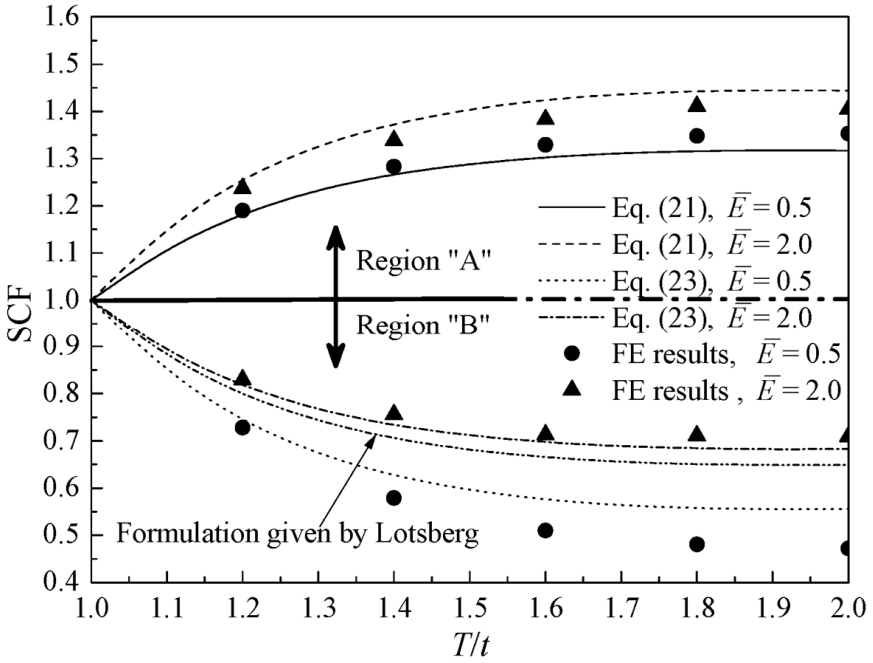

Figure 10. Comparison of SCFs from present formulations and FE analysis for $\bar{t} = 0.5$.

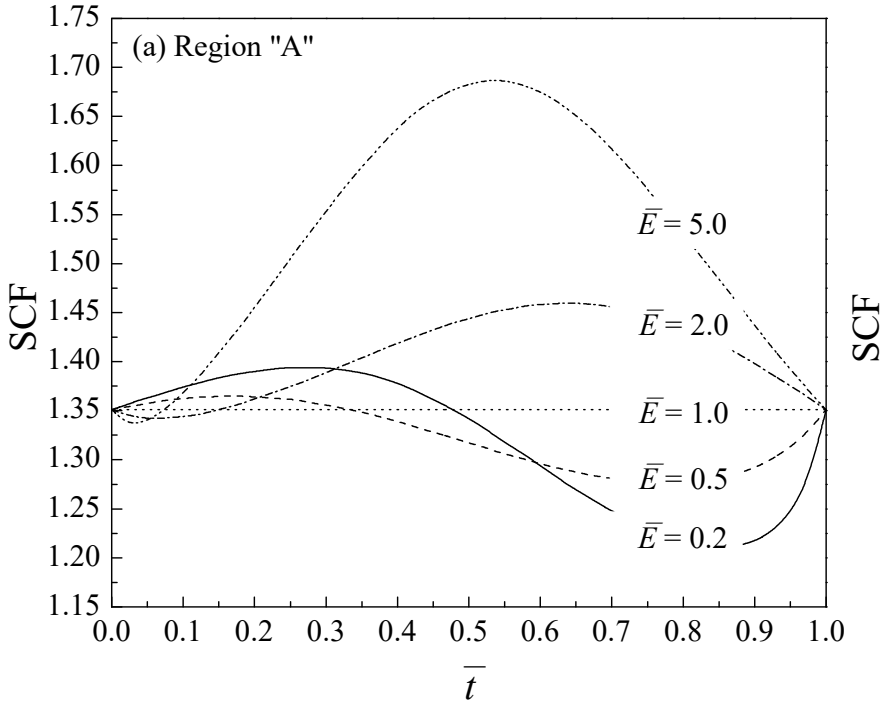

Figure 11. *Cont.*

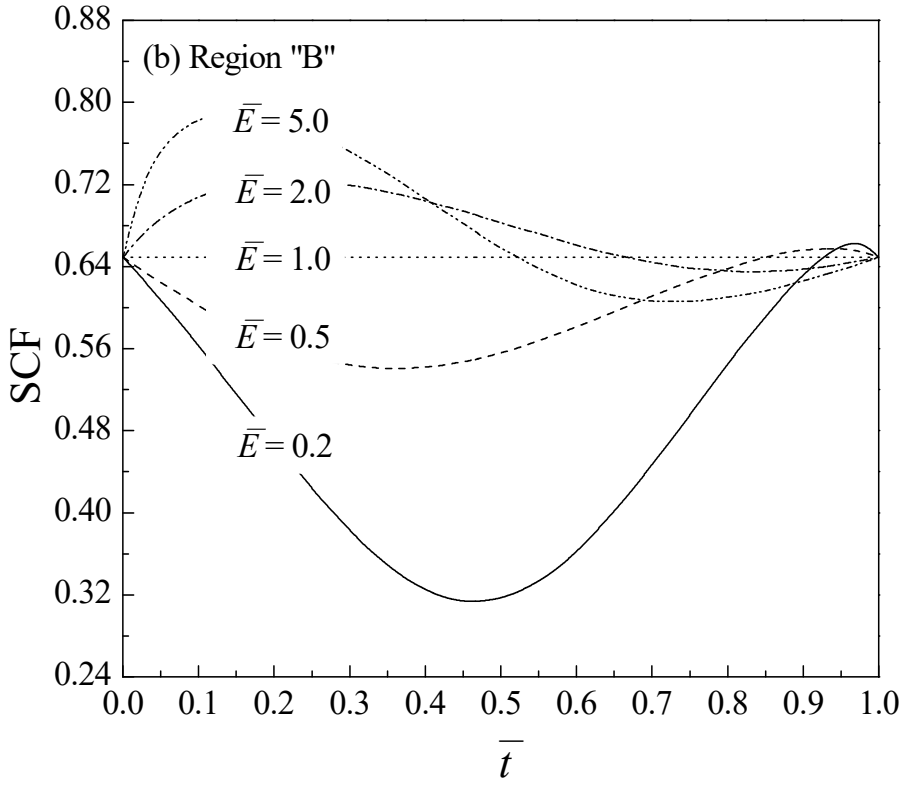

Figure 11. Effect of $\overline{E}$ on SCFs over $\overline{t}$ for $T/t = 2.0$.

5. Conclusions

The present study investigates the effect of fabrication tolerances and thickness transitions on the SCFs for girth welds in a bi-layer pipe. Based on the classical shell theory [14], the governing equation of a bi-layer cylindrical shell subjected to an axial force and an internal pressure is built up. Then, the equation is used to derive SCF formulations for girth welds of a bi-layer pipe with fabrication tolerances and thickness transitions. Axisymmetric FE analysis is carried out to validate the proposed formulations, and a good agreement between the formulation and the FE results is observed. These formulations are well suited for a wide range of thickness ratios $\overline{t}$ and elastic modulus ratios $\overline{E}$, and degraded to the expressions derived by Lotsberg [10] when $\overline{t} = 0$ or $\overline{E} = 1$. Finally, the influence of varying $\overline{t}$ and $\overline{E}$ on the SCF are investigated in detail.

Author Contributions: Conceptualization, Y.Z. and H.Z.; methodology, H.Z.; software, H.H.; validation, R.G. and H.H.; formal analysis, R.G. and H.H.; investigation, R.G. and H.H.; resources, Y.Z. and H.Z.; data curation, R.G. and H.H.; writing—original draft preparation, H.H. and H.Z.; writing—review and editing, R.G. and Y.Z.; visualization, H.Z.; supervision, Y.Z. and H.Z.; project administration, R.G.; funding acquisition, R.G. All authors have read and agreed to the published version of the manuscript.

Funding: This research was funded by the Scientific Research Foundation of the Wuhan Institute of Technology, grant number 21QD37.

Institutional Review Board Statement: Not applicable.

Informed Consent Statement: Not applicable.

Data Availability Statement: The data presented in this study are available on request from the corresponding author.

Conflicts of Interest: The authors declare no conflicts of interest.

Appendix A

This appendix details the derivation of the governing equation for the bi-layer cylindrical shell subjected to an internal pressure $p(x)$ and an axial force N uniformly distributed along the x-direction, as shown in Figure 1. The total thickness of the shell is denoted by t, this quantity always being considered small compared to other dimensions of the shell. The neutral surface is the surface free of stress when a shell is loaded by a bending force, and the surface that bisects the thickness of the shell is named the middle surface. For the one-layer shell, it is noted clearly that the neutral surface is overlapped with the middle surface. However, the neutral surface of the bi-layer shell deviates from the middle surface due to the variation of material properties along the thickness direction. Therefore, it is necessary to determine the position of the neutral surface in order to derive the final governing equation.

Due to t being very small in comparison with the radius of the shell as referred to above, the infinitely small element (Figure A1a) cut from the shell can be regarded as a rectangular one (Figure A1b), and the small rectangular element follows the Kirchhoff assumptions [13] during the action of symmetric loadings. Therefore, the strain along the x-direction is distributed linearly, as indicated in Figure A1c, along the thickness direction, and it can be expressed as:

$$\varepsilon_x = \frac{\varepsilon_t}{t/2 - \eta_n}\eta \tag{A1}$$

where ε_t is the x-direction strain at the top of the element, η is the vertical coordinate in the local ξ-η coordinate system, η_n denotes the vertical coordinate of the neutral surface. It is noteworthy that if the ratio of thickness to radius cannot be neglected, the above assumption may not be valid.

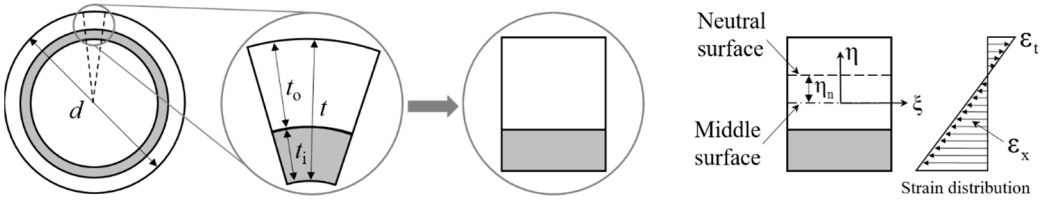

Figure A1. Schematics of small element cut from shell cross-section.

In this study, it is assumed that the shell's outer and inner layers have the same Poisson's ratio ($v_o = v_i = v$) but different elastic modulus ($E_o \neq E_i$). The position of the neutral surface can be determined based on the x-direction equilibrium of forces, and the integral expression is written as:

$$\int_0^{t/2-\eta_n} E_o \varepsilon_x \mathrm{d}\eta = \int_{-(t/2+\eta_n)}^{-(t/2+\eta_n)+t_i} E_i \varepsilon_x \mathrm{d}\eta + \int_{-(t/2+\eta_n)+t_i}^{0} E_o \varepsilon_x \mathrm{d}\eta \tag{A2}$$

By solving the above integral, η_n is expressed in the following form:

$$\eta_n = \overline{\eta}_n t \tag{A3}$$

where

$$\overline{\eta}_n = \frac{\overline{t}(1-\overline{t})(1-\overline{E})}{2(1-\overline{t}+\overline{t}\overline{E})}, \quad \overline{t} = t_i/t, \quad \overline{E} = E_i/E_o \tag{A4}$$

and $\overline{t}$ indicates the ratio of the inner layer thickness to the total thickness, and $\overline{E}$ is the ratio of the inner layer elastic modulus to that of the outer layer, both characterizing the bi-layer shell, which is different from the one-layer one.

In the following, the governing equation of the bi-layer shell is built up under an axial force and an internal pressure. An infinitely small element (Figure A2) cut from the shell is analyzed to establish the equations of equilibrium required for this problem. N_x and N_φ are the axial forces per unit circumferential length and per unit length around the circumference of the shell, respectively, Q_x is the shear force per unit circumferential length, M_x and M_φ are the bending moments per unit circumferential length and per unit length around the circumference of the shell, respectively. Due to symmetry, other forces such as $N_{x\varphi}$, Q_φ and $M_{x\varphi}$ vanish in this case. Assuming that an internal pressure $p(x)$ normal to the surface and an axial force N uniformly distributed along the x-direction are applied, the equations of equilibrium obtained are:

$$\begin{gathered} N_x = N \\ \frac{dQ_x}{dx} + \frac{1}{r}N_\varphi = -p(x) \\ \frac{dM_x}{dx} - Q_x = 0 \end{gathered} \tag{A5}$$

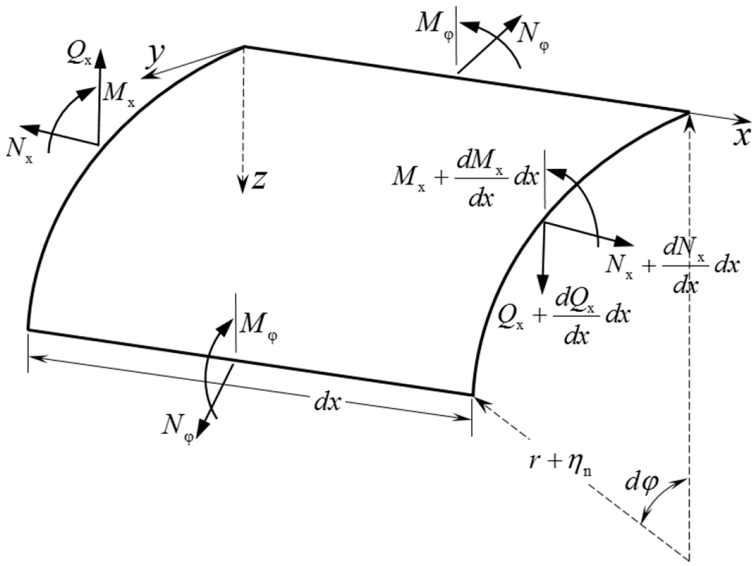

Figure A2. An infinitely small shell element used in the analysis.

The displacements of the points in the neutral surface of the shell need to be considered to solve the other three unknown quantities: N_φ, Q_x, and M_x. From symmetry, the displacement component v in the circumferential direction vanishes. The components u and w in the x- and z- directions are only considered. Therefore, the geometric equations can be written in the following simplified form:

$$\varepsilon_x = \frac{\mathrm{d}u}{\mathrm{d}x}, \quad \varepsilon_\varphi = -\frac{w}{r} \tag{A6}$$

By using Hooke's law,

$$\sigma_x = \frac{E}{1-v^2}(\varepsilon_x + v\varepsilon_\varphi), \quad \sigma_\varphi = \frac{E}{1-v^2}(\varepsilon_\varphi + v\varepsilon_x) \tag{A7}$$

and the relationship between N_x, N_φ, Q_x, M_x and σ_x, σ_φ,

$$N_x = \int_0^t \sigma_x \mathrm{d}\eta, \quad N_\varphi = \int_0^t \sigma_\varphi \mathrm{d}\eta, \quad M_x = \int_{-t/2-\eta_n}^{t/2-\eta_n} \sigma_x \eta \mathrm{d}\eta \tag{A8}$$

the constitutive equations for this problem are:

$$\begin{aligned} N_x &= \alpha_1 \frac{du}{dx} - \alpha_2 \frac{w}{r} \\ N_\varphi &= -\alpha_1 \frac{w}{r} + \alpha_2 \frac{du}{dx} \\ M_x &= -D_b \frac{d^2 w}{dx^2} \end{aligned} \tag{A9}$$

where

$$\alpha_1 = \frac{\left(1 - \bar{t} + \bar{t}\bar{E}\right) t E_o}{1 - v^2}, \quad \alpha_2 = \frac{\left(1 - \bar{t} + \bar{t}\bar{E}\right) t E_o v}{1 - v^2} \tag{A10}$$

and D_b is the flexural rigidity of the bi-layer shell, which is expressed as:

$$D_b = \frac{E_o t^3}{24(1 - v^2)} \left[(1 - 2\bar{\eta}_n)^3 + \bar{E}(1 + 2\bar{\eta}_n)^3 + \left(1 + 2\bar{\eta}_n - 2\bar{t}\right)^3 - \bar{E}\left(1 + 2\bar{\eta}_n - 2\bar{t}\right)^3 \right] \tag{A11}$$

Substituting Equation (A9) into Equation (A5) obtains the required governing equations,

$$\frac{\mathrm{d}^2}{\mathrm{d}x^2} \left(D_b \frac{\mathrm{d}^2 w}{\mathrm{d}x^2} \right) + \frac{\alpha E_o t}{r^2} w = p(x) - \frac{v}{r} N \tag{A12}$$

where

$$\alpha = 1 - \bar{t} + \bar{t}\bar{E} \tag{A13}$$

When the thickness of the shell is constant, the above equation is simplified as:

$$D_b \frac{\mathrm{d}^4 w}{\mathrm{d}x^4} + \frac{\alpha E_o t}{r^2} w = p(x) - \frac{v}{r} N \tag{A14}$$

Obviously, the form of the equation is nearly the same as that of the one-layer shell except for the expressions of the flexural rigidity D_b and the dimensionless parameter α. When $\bar{t} = 0$ or $\bar{E} = 1$, $D_b = Et^3/12(1 - v^2)$ and $\alpha = 1$, and Equation (A14) becomes the governing equation for the one-layer shell derived based on the classical shell theory.

Appendix B

This appendix focuses on the generation of FE models for bi-layer pipelines with misalignment at girth welds, including a detailed description on the number of elements, types of elements, element sizes, loads, boundary conditions, and the overall structure of the finite element mesh. Moreover, it outlines the procedural steps and critical considerations in the generation of FE models.

Firstly, the FE model of bi-layer pipe without misalignment should be generated, which is actually not difficult in practice because the shape of bi-layer pipe is quite regular. Figure A3 shows the typical FE meshes of the girth weld.

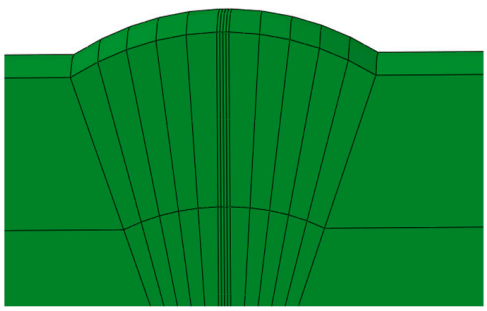

Figure A3. Typical FE meshes at the girth weld.

Then, the coordinate transformation was adopted to generate FE models of bi-layer pipelines with misalignment at girth welds from the FE model of aligned bi-layer pipelines. The coordinate transformation formulas presented below are essential for adapting aligned pipeline models to accommodate misalignments, reflecting more realistic and complex real-world scenarios. This addition enhances the applicability of the finite element method in pipeline structural and stress analysis, allowing for more accurate simulations and analyses of pipelines under various conditions, including those that are not perfectly aligned. Figure A4a,b illustrates the coordination transformation of bi-layer pipe, which has centerline offset with equal thickness and diameters and bi-layer pipe, which has centerline offset with varying thickness but aligned inner surfaces, respectively.

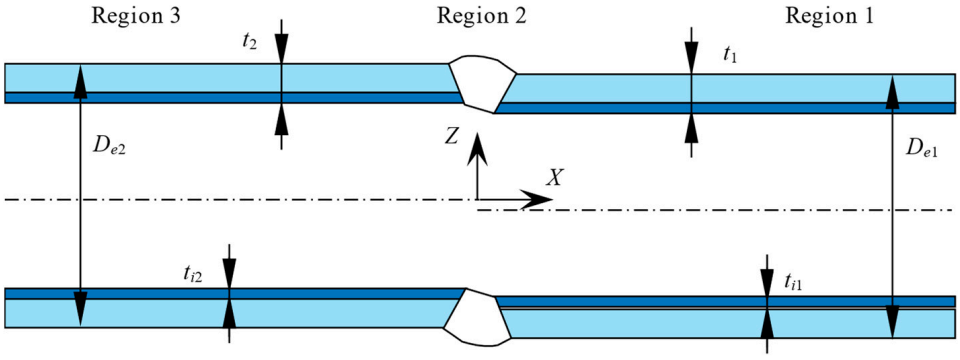

(a) Bi-layer pipe having centerline offset with equal thickness and diameters

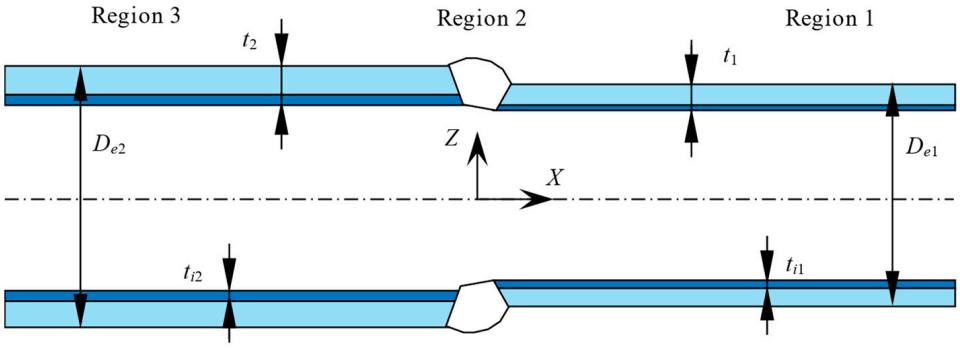

(b) Bi-layer pipe having centerline offset with varying thickness but aligned inner surfaces

Figure A4. Coordinate transformation of typical bi-layer pipes with misalignment.

For bi-layer pipe with a centerline offset with equal thickness and diameters (Figure A4a), the transformation from an aligned (x-, y-, z- coordinate system) to a misaligned configuration (X-, Y-, Z- coordinate system) is executed using the specified expression as follows.

$$\text{Region 1} \begin{cases} X = x \\ Y = y \\ Z = z - e \end{cases} \tag{A15a}$$

$$\text{Region 2} \begin{cases} X = x \\ Y = y \\ Z = z - e_{\text{eff}} \end{cases} \tag{A15b}$$

$$\text{Region 3} \quad \begin{cases} X = x \\ Y = y \\ Z = z \end{cases} \tag{A15c}$$

where

$$e_{\text{eff}} = \left(\frac{2x + L_{\text{e}} + L_{\text{v}}}{2L_{\text{v}}} \right) e \tag{A16}$$

$$L_{\text{v}} = L_{\text{i}} + \frac{[2(r + t_2) - D_{\text{e2}}](L_{\text{e}} - L_{\text{i}})}{2t_2} \tag{A17}$$

$$r = \sqrt{y^2 + z^2} \tag{A18}$$

For a bi-layer pipe with a centerline offset with varying thickness but aligned inner surfaces (Figure A4b), there are two scenarios: $r \leq r_{\text{c}}$ and $r > r_{\text{c}}$ with $r_{\text{c}} = D_{\text{e2}}/2 - (t_2 - t_{\text{i2}})$. Here, t_{i2} represents the clad layer thickness, as shown in Figure A4b. The coordinate transformation for these two cases is summarized through specific expressions as follows.

For the first scenario, $r \leq r_{\text{c}}$:

$$\text{Region 1} \quad \begin{cases} X = x \\ Y = (r - e_{v1})\sin\theta \\ Z = (r - e_{v1})\cos\theta \end{cases} \tag{A19a}$$

$$\text{Region 2} \quad \begin{cases} X = x \\ Y = (r - e_{v1,\text{eff}})\sin\theta \\ Z = (r - e_{v1,\text{eff}})\cos\theta \end{cases} \tag{A19b}$$

$$\text{Region 3} \quad \begin{cases} X = x \\ Y = y \\ Z = z \end{cases} \tag{A19c}$$

where

$$e_{v1} = (t_{i2} - t_{i1}) \left[\frac{r - (D_{e2}/2 - t_2)}{t_{i2}} \right] \tag{A20}$$

$$e_{v1,eff} = \left(\frac{2x + L_e + L_v}{2L_v} \right) e_{v1} \tag{A21}$$

For the second scenario, $r > r_{\text{c}}$:

$$\text{Region 1} \quad \begin{cases} X = x \\ Y = (r - e_{v2})\sin\theta \\ Z = (r - e_{v2})\cos\theta \end{cases} \tag{A22a}$$

$$\text{Region 2} \quad \begin{cases} X = x \\ Y = (r - e_{v2,\text{eff}})\sin\theta \\ Z = (r - e_{v2,\text{eff}})\cos\theta \end{cases} \tag{A22b}$$

$$\text{Region 3} \quad \begin{cases} X = x \\ Y = y \\ Z = z \end{cases} \tag{A22c}$$

where

$$e_{v2} = (t_{i2} - t_{i1}) + \left(1 - \frac{t_1 - t_{i1}}{t_2 - t_{i2}}\right)(r - r_c) \tag{A23}$$

$$e_{v2,\text{eff}} = \left(\frac{2x + L_e + L_v}{2L_v}\right) e_{v2} \tag{A24}$$

Consequently, the FE models of the two typical bi-layer pipes with misalignment can be generated, which can be seen in Figure A5.

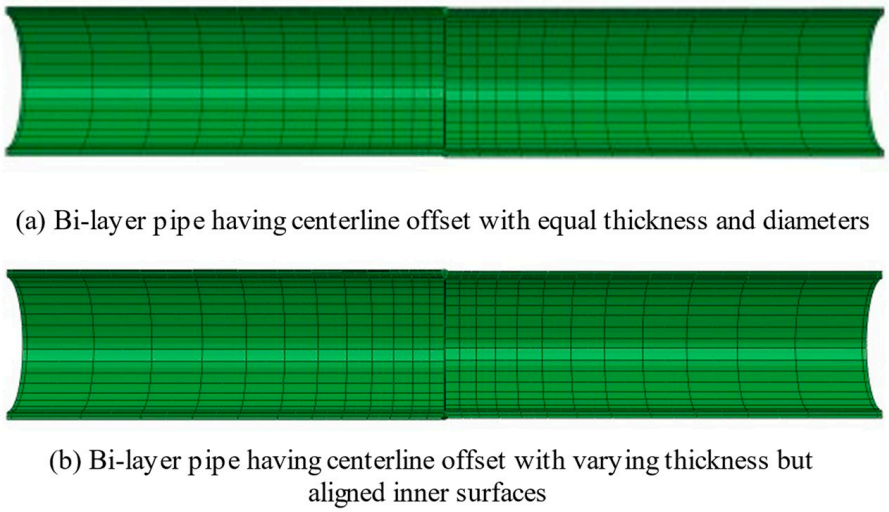

(a) Bi-layer pipe having centerline offset with equal thickness and diameters

(b) Bi-layer pipe having centerline offset with varying thickness but aligned inner surfaces

Figure A5. FE models of typical bi-layer pipes with misalignment.

The FE models in this study were generated using the ABAQUS software V2021. Given the consideration of large deformations, the C3D20R element is used for the numerical simulation. It is difficult to determine the mesh density directly; hence, the convergence test is recommended to determine the number of elements in the FE models. One can gradually increase the mesh density until the simulation results converge. In this study, the number of elements increases to 1×10^4 to make the results converge. In addition, the axial force is applied at one end of the pipe, and the fixed boundary condition is applied on the other.

References

1. Marshall, P.W. A review of stress concentration factors in tubular connections. In *Report CE-32*; Shell: Houston, TX, USA, 1978.
2. Zavvar, E.; Henneberg, J.; Soares, C.G. Stress concentration factors in FRP-reinforced tubular DKT joints under axial loads. *Mar. Struct.* **2023**, *90*, 103429. [CrossRef]
3. Bao, S.; Wang, W.; Li, X.; Zhou, J. Stress concentration factor distribution formulas for three-planar tubular Y-joints under axial force. *Ocean. Eng.* **2022**, *265*, 112687. [CrossRef]
4. Nassiraei, H.; Rezadoost, P. Stress concentration factors in tubular T-joints reinforced with external ring under in-plane bending moment. *Ocean. Eng.* **2022**, *266*, 112551. [CrossRef]
5. Sofiani, F.M.; Chaudhuri, S.; Elahi, S.A.; Hectors, K.; De Waele, W. Quantitative analysis of the correlation between geometric parameters of pits and stress concentration factors for a plate subject to uniaxial tensile stress. *Theor. Appl. Fract. Mech.* **2023**, *127*, 104081. [CrossRef]
6. Brabin, T.A.; Christopher, T.; Rao, B.N. Finite element analysis of cylindrical pressure vessels having a misalignment in a circumferential joint. *Int. J. Press. Vessel. Pip.* **2010**, *87*, 197–201. [CrossRef]
7. Maddox, S.J. *Fitness for Purpose Assessment of Misalignment in Transverse Butt Welds Subjected to Fatigue Loading*; IIW Document XIII-1180; International Institute of Welding: Genoa, Italy, 1985.
8. Efthymiou, M. Development of SCF formulae and generalised influence functions for use in fatigue analysis. In *Recent Developments in Tubular Joint Technology*; OTJ'88: London, UK, 1988.
9. Smedley, S.; Fischer, P. Stress concentration factors for ring-stiffened tubular joints. In Proceedings of the 1st International Offshore and Polar Engineering Conference, Edinburgh, UK, 11–16 August 1991.
10. Lotsberg, I. Stress concentration factors at circumferential welds in tubulars. *Mar. Struct.* **1998**, *11*, 203–230. [CrossRef]
11. Lotsberg, I. Stress concentration factors at welds in pipelines and tanks subjected to internal pressure and axial force. *Mar. Struct.* **2008**, *21*, 138–159. [CrossRef]

12. Lotsberg, I. Stress concentrations due to misalignment at butt welds in plated structures and at girth welds in tubulars. *Int. J. Fatigue* **2009**, *31*, 1337–1345. [CrossRef]
13. Timoshenko, S.P.; Woinowsky-Krieger, S. *Theory of Plates and Shells*, 2nd ed.; McGraw-Hill Book Company, Inc.: New York, NY, USA, 1959.
14. *DNV-RP-C203*; Fatigue Design of Offshore Steel Structures. Det Norske Veritas AS: New York, NY, USA, 2011.
15. *BS7910-Amendment 1*; Guide to Methods for Assessing the Acceptability of Flaws in Metallic Structures. British Standards Institution: Jersey, UK, 2013.
16. Zhao, H.S.; Lie, S.T.; Zhang, Y. Stress intensity factors for semi-elliptical surface cracks in plate-to-plate butt welds with parallel misalignment of same thickness. *Mar. Struct.* **2017**, *53*, 148–163. [CrossRef]
17. Yi, D.; Xiao, Z.M.; Idapalapati, S.; Kumar, S.B. Fracture analysis of girth welded pipelines with 3D embedded cracks subjected to biaxial loading conditions. *Eng. Fract. Mech.* **2012**, *96*, 570–587. [CrossRef]
18. Chang, Q.; Cao, Y.G.; Zhen, Y.; Wu, G.; Li, F.G. Study on the effect of loading conditions on the fracture behavior of pipeline with girth weld. *Int. J. Press. Vessel. Pip.* **2023**, *203*, 104940. [CrossRef]
19. Cao, Y.G.; Chang, Q.; Zhen, Y. Numerical simulation of fracture behavior for the pipeline with girth weld under axial load. *Eng. Fail. Anal.* **2022**, *136*, 106221. [CrossRef]
20. Gong, B.M.; Wan, X.B.; Huo, X.T.; Liu, Y.; Deng, C.Y.; Wang, D.P.; Dai, L.S. Development of a strain-based fracture assessment approach for X80 steel pipe welded girth by modified Mohr-Coulomb model. *Int. J. Press. Vessel. Pip.* **2023**, *206*, 105056. [CrossRef]
21. Zhao, H.S.; Lie, S.T.; Zhang, Y. Elastic-plastic fracture analyses for misaligned clad pipeline containing a canoe shape surface crack subjected to large plastic deformation. *Ocean. Eng.* **2017**, *146*, 87–100. [CrossRef]
22. Zhang, Y.H.; Shuai, J.; Lv, Z.Y.; Zhang, T.Y. Study on fracture behavior of pipeline girth weld based on CTOD-Am method and Gurson ductile damage model. *Theor. Appl. Fract. Mech.* **2023**, *123*, 103692. [CrossRef]
23. Zhao, H.S.; Hu, Y.Y.; Bi, C.W.; Li, X. Numerical study on hydrodynamic behaviors of and flow field around UHMWPE plane nets. *Aquac. Eng.* **2024**, *106*, 102397. [CrossRef]